Bützer, T., Vigaru, B., and Gassert, R. (2015). Design and evaluation of a compact, integrated fMRI-compatible force sensor printed by additive manufacturing. IEEE World Haptics Conference, pp. 158-164.
2015 IEEE World Haptics Conference (WHC)
Northwestern University
June 22–26, 2015. Evanston, Il, USA

Design and Evaluation of a Compact, Integrated fMRI-Compatible Force Sensor Printed by Additive Manufacturing

Tobias Bützer*, Bogdan Vigaru*, and Roger Gassert

***Abstract*— The past decade has seen an increasing number of motor control studies using functional magnetic resonance imaging to explore the underlying neural mechanisms. To enable advanced experimental paradigms under well-controlled and reproducible conditions, a number of fMRI-compatible haptic interfaces have been developed for such studies. These devices typically rely on actuation principles and transmissions with non-linear behavior and large output impedance. Fiberoptic force sensors are a common and well-established means of measuring interaction forces with subjects or to reduce the inherent dynamics of the haptic interface through force feedback. The elastic probes for such sensors are typically fabricated by expensive methods such as electro-erosion of non-ferromagnetic metals or injection moulding of polymers, or are realized by milling of polymers, resulting in bulky structures. In this paper we propose a compact and integrated elastic probe for fiberoptics-based force sensing, developed using low-cost off-the-shelf 3D printing technology. Characterization of the sensor probe shows high linearity, repeatability and temporal stability, as well as high reproducibility in terms of the manufacturing process. The realized sensor is integrated into a linear grasper to evaluate its performance in force-feedback applications, underlining the potential of this technology for use in fMRI-compatible haptic interfaces.**

I. INTRODUCTION

The interest in functional magnetic resonance imaging (fMRI) based research on human motor control has increased rapidly over the past few years. To enable advanced experimental paradigms under well-controlled and reproducible conditions, a number of fMRI-compatible haptic interfaces have been developed for such studies, capable of controlling the interaction with arm [1]–[4] or finger/hand movements [5]–[7]. Along with these devices, the development of (f)MRI-compatible actuation and sensing components has been required. Force sensors are of particular interest, as they allow measuring interaction forces with a subject, or can be used to reduce the apparent dynamics of a haptic interface through force feedback.

Various sensing principles have been investigated for fMRI-compatible force sensors (for an overview see [8]). Liu et al. developed a grip dynamometer based on remote pressure measurement via a hydraulic transmission [9], and Hidler et al. built a custom non-magnetic 6-axis load cell [10] in order to achieve fMRI compatibility. Special interest, however, have received fiberoptic sensors due to their inherent compatibility with the MRI environment. Hirose and Yoneda were among the first to develop a force sensor using fiberoptics technology [11], while Tada et al. modified the design to make it usable in the MRI environment [12]. More recent developments in this field can be found in [13], [14].

All aforementioned fiberoptic sensors rely on displacement measurements of flexible structures, i.e. the deformation of an elastic probe under the application of an external force. These flexible structures are mostly either realized by electro-erosion of non-ferromagnetic metals as in [13], or by milling of polymers as in [15]. The former method has the disadvantage of being rather expensive and also susceptible to eddy currents, which results in resistive forces when moved in the spatial gradient of the static magnetic field of the MRI scanner, while the latter can result in bulky structures. In this paper we propose an fMRI-compatible fiberoptics-based force sensor employing off-the-shelf technology such as a fiberoptic sensor and amplifier, and an integrated elastic probe fabricated by low-cost 3D printing technology. It carries the advantage of fast and affordable production and reproduction, the absence of ferromagnetic components, and the ability to easily adapt the probe to the specific needs of a given application and integrate it with neighboring components. In section II we focus on the application for which the sensor is designed, specify the requirements for the development of such a sensor, and describe the used manufacturing tools and off-the-shelf components. Section III describes the flexible structure, while section IV presents methods and results of the sensor characterization. Finally, advantages and limitations of the developed sensor are discussed in section V.

II. SENSOR REQUIREMENTS

A. Targeted Application

While the sensor design proposed in this paper can be adapted to various applications, it was developed for a scenario in which a human subject performs precision grip movements (moving index finger while the thumb is fixed) against virtual dynamic loads during fMRI. To ensure good dynamic performance, we assume a setup consisting of a shielded electromagnetic motor placed at some distance from the scanner bore [16], which actuates a mobile finger module guided by a linear friction slide through a capstan and closed cable loop in direct-drive mode. For evaluation purposes within the scope of this paper and to derive the design requirements, the device presented in Fig. 10 was used as a representative setup. This device suffers from static friction in the linear guide and the pulley loaded by the pretensioned cable transmission, which can only be compensated through force feedback. The goal was therefore to design and develop

The authors are with the Rehabilitation Engineering Laboratory, ETH Zurich, 8092 Zurich, Switzerland {tbuetzer,vigarub,gassertr}@ethz.ch
* These authors contributed equally to this work.

a compact force sensor with a small linear range ($\pm 2\ N$) that could be easily integrated into such a device to reduce the static friction. The design should be as compact as possible, and integrate the surrounding components, such as the finger fixation and the attachment to the linear guide. Note that the sensor is designed to deflect within the range of the static friction of the device, and to then hit a mechanical stop once this force is overcome, as the interaction force can then be estimated from motor currents while considering a viscous friction model. The elastic probe should thus support overload forces in the range of human finger pinching, i.e. up to 40 N [17].

B. fMRI-Compatibility

To guarantee fMRI-compatibility, several constraints imposed by the MRI environment with respect to the use of robotic devices have to be respected:

- Current MRI scanners produce a static magnetic field of 3 T (Tesla). This prohibits the use of ferromagnetic materials, which would be accelerated within the spatial gradient associated with the magnetic field generated by the scanner (missile effect).
- The use of electrically conducting materials should additionally be minimized. If placed at the entry of the scanner bore (i.e. within the fringe field), eddy currents will be induced in moving parts, leading to thermal and mechanical effects which can disturb the imaging. This effect can also be caused by the switching magnetic field gradients of the scanner.
- In order to allow force measurement during fMRI image acquisition, the sensor must not disturb the imaging and at the same time be insensitive to the static magnetic field, static and switching magnetic field gradients and radio frequency pulses generated by the scanner.
- The space requirements for robotic systems to be used within an MR scanner are particularly stringent as the scanner bore is a narrow tube of about 60–70 cm in diameter and occupied mostly by the subject. Additionally, sensors often need to be integrated into the mechanical structures, and their size/shape must be adapted to the dimensions of the structure.

C. Materials: Fiberoptic Sensor and 3D Printer

We chose a commercial fiberoptic sensor (Baumer Electric, Switzerland, detailed specifications presented in Table I) based on its proven reliability in earlier developments [13], [15]. As illustrated in Fig. 1, this sensor is composed of an fMRI-compatible sensor head (brass), an analog amplifier (non-fMRI-compatible), and two optical fibers of 10 m length connecting the two components. It is an optical distance sensor and it's working principle is based on measuring reflected light intensity (Fig. 2): one sensor channel emits light through the optical fiber, a mirror attached to the flexible probe reflects this light with the reflected intensity depending on the deflection of the probe, while the other sensor channels the reflected light back to the amplifier. The change of measured light intensity thus results in a variation of the output voltage of the analog amplifier. Force can therefore be measured through the displacement of the mirror on the flexible probe, which deforms under the application of this force. As the linear range of this fiberoptic sensor is 0.6 mm (distance between sensor head and mirror), a requirement for the design of the force sensor is that the deformation of the flexible probe should be less than $\pm 0.3\ mm$ under maximum desired compression/traction load to ensure linearity.

Two of the disadvantages of previously developed fiberoptics-based force sensors [13], [15] are the rather high production times and costs, as well as the bulkiness and limited complexity of milled polymer structures. We aimed to overcome these by using a low-cost 3D printer (MakerBot Replicator 2, MakerBot, USA). It fabricates 3D parts layer-by-layer by extruding PLA (polylactic acid), a biodegradable thermoplastic through a heated nozzle. The use of this technology enables not only fast and affordable production of sensor probes, but also guarantees MRI compatibility while allowing to adapt the design to the requirements of the application at hand (e.g. in terms of dimensions and measurement range) and to the surrounding mechanical components.

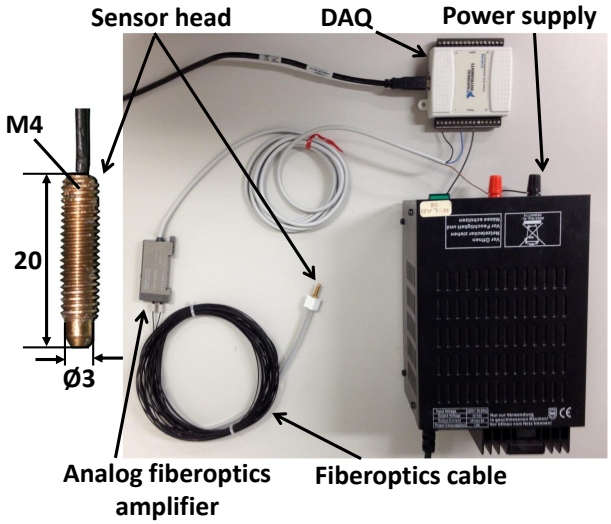

Fig. 1. Fiberoptic sensor components, USB data acquisition card (DAQ) and power supply.

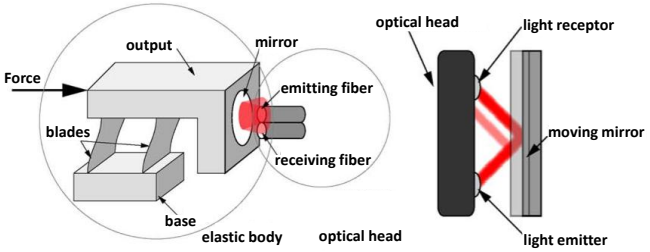

Fig. 2. Reflected light intensity measurement (reprinted from [15]). (left) Flexible structure deforming under the application of an external force. (right) Change in reflected light intensity with displacement of the mirror.

TABLE I

FIBEROPTICS SENSOR, DAQ AND POWER SUPPLY SPECIFICATIONS.

Sensor head	FUE999C1004
Sensor amplifier	FWDK 10U84Y0
Cable length	10 m
Linear sensing distance	0.6 mm
Light source	Pulsed red LED
Wave length	680 nm
Response time	1 to 50 ms
Sensor head size	$\phi 4 \times 20$ mm
Sensor amplifier size	$10 \times 29.7 \times 60$ mm^3
Data acquisition card	National Instruments USB 6008, 12 bit
Power supply	Voltcraft FSP 1243, 24 VDC

III. DESIGN AND IMPLEMENTATION

A. Mechanical Structure

We designed a flexible structure based on a simple compliant mechanism consisting of a fixed base and a deflecting probe connected through two flexible hinges, as illustrated in Fig. 3. When force *P* is applied along a horizontal direction, the flexible hinges deform elastically and the probe translates by f along the direction of the applied force. According to Henein [18], the relation between applied force *P* and the displacement f of the elastic probe is given by:

$$f = \frac{P}{2K} \tag{1}$$

with

$$K = \frac{12EI_y}{l^3} \tag{2}$$

and

$$I_y = \frac{bh^3}{12} \tag{3}$$

where *K* is the rigidity of a single hinge along the direction of force P, I_y is the moment of inertia, E is Young's modulus (2400 MPa[1]) and l, h, b are the length, thickness and width of the hinges, respectively. Henein further proposes design constraints to minimize the effect of transverse forces. For

$$\frac{l}{h} > 10 \tag{4}$$

and

$$\frac{b}{h} > 10 \tag{5}$$

the rigidities in directions transverse to the direction of force P and the rigidities for torsion in all directions are significantly higher than the rigidity in the expected force direction (factor 100) and can be considered as locked along these directions. The parasitic displacement λ is described by:

$$\lambda = \frac{3f^2}{5l} \tag{6}$$

and can be neglected if

$$\frac{l}{f} > 30 \tag{7}$$

[1]Yield-stress and Young's moduli of polymeric materials such as PLA are strongly temperature-dependent [19].

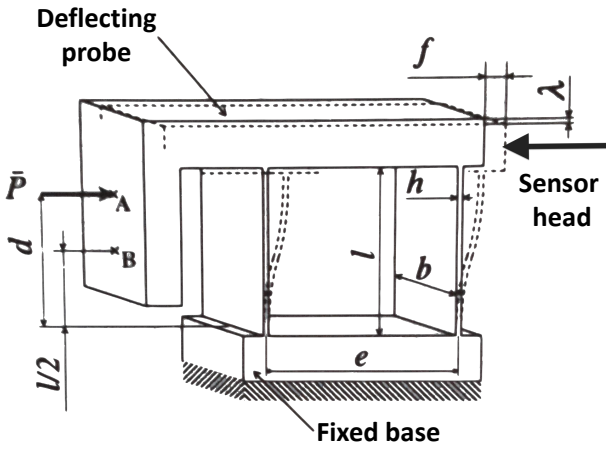

Fig. 3. Flexible structure of sensor prototype (adapted from [18]). Applied force point and sensor head placement are indicated.

In order to achieve the smallest possible size using the selected fabrication method, we determined the thinnest hinge that could be printed repeatedly with consistent results to be $h = 0.08$ mm. Using equations (1–3), the flexible hinges were designed to meet the desired force sensing range, i.e. a maximum displacement of the flexible probe of $\pm$ 0.3 mm when the maximum force of $\pm$ 3 N is applied. Considering equations (4–7), the dimensions of the flexible hinges were 0.8 mm (h) $\times$ 14 mm (l) $\times$ 10 mm (b).

To prevent large deformations of the flexible hinges at high forces (force overload), which would result in plastic deformation, a frame with mechanical stops on either side was designed. The mechanical stops limit the range of motion (ROM) of the deflecting probe to $\pm$ 0.25 mm, rather than to the full linear range of $\pm$ 0.3 mm of the fiberoptic sensor. Contact between the mirror and the sensor head is thereby prevented. Additional stiffness for the frame is provided by a layer of PLA running beneath the elastic probe and connecting the two sides of the frame.

The force sensor does not only need to achieve the desired sensing range, but a linear behavior and repeatable output are also crucial for its application. The flexible hinges must therefore not undergo plastic deformation. From equations (1–3), and the design parameters l, b, h we can derive the theoretical stiffness of the flexible structure as

$$\frac{f}{P} = \frac{l^3}{2bh^3E} = 0.11mm/N \tag{8}$$

A finite element method analysis (FEM; using Pro/ENGINEER Wildfire 4.0 Mechanica; PTC, USA) yielded a stiffness of 0.08 mm/N, which corresponds much better to the experimentally determined stiffness of the printed probe (see section IV-A). Further FEM analysis revealed a highly linear displacement behavior. The maximum stress at the maximum displacement (i.e. where the deflecting probe contacts the mechanical stops) was calculated to be 11.25 MPa, as illustrated in Fig. 4. As this is below the maximal yield stress of PLA (25 MPa [19]), the flexible structure is only deformed elastically.

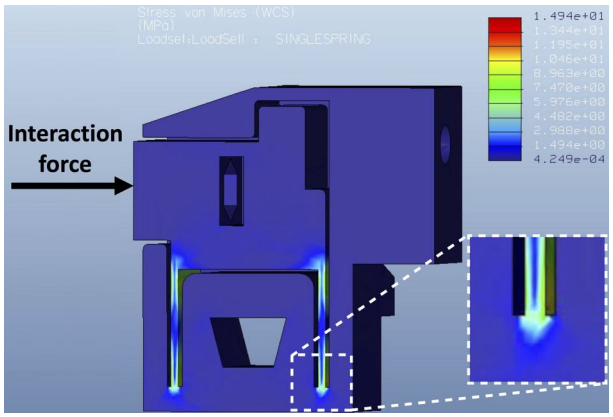

Fig. 4. FEM analysis showing the stress distribution in the flexible structure when force is applied. The maximum stress (zoomed-in area) at maximum deformation is 11.25 MPa (maximal yield stress of PLA: 25 MPa [19]).

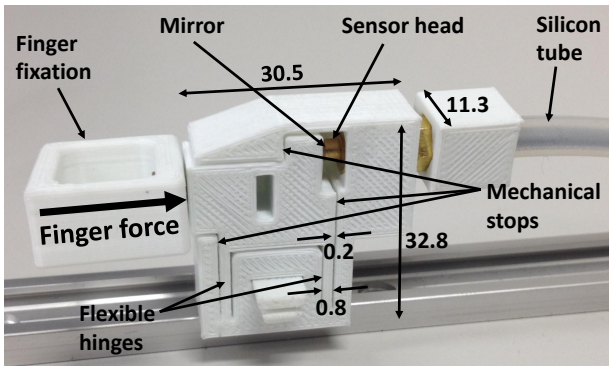

Fig. 5. Integrated fiberoptic force sensor assembly, consisting of an elastic probe with mechanical overload protection (mechanical stops), a fixation block for the optical fiber with a silicon tube to prevent extensive bending of the fibers at the interface to the probe, a finger module with a free rotational DOF, and a clip-on mechanism to attach the sensor assembly to the carriage of a linear guide.

B. Assembled Force Sensor

The final design is illustrated in Fig. 5. It shows the mirror attached to the deflecting structure, the flexible hinges, the sensor head facing the mirror and the mechanical stops. The dimensions of the force sensor are 30.5 $\times$ 32.8 $\times$ 11.3 mm^3 and weighs 9 g. The offset of the mirror from the center of the probe provides a higher surface for the mechanical stops on either side. Due to the parallel movement of the entire deflecting probe, displacement of the mirror is not affected by this offset. The fiberoptic cable is wrapped by a silicon tube to prevent excessive bending at the attachment point, which could lead to undesired voltage drops. As threaded holes cannot be 3D-printed into the material, the sensor head is fixed with brass nuts on either side, which are press-fitted into holes in the sensor structure. Together with the sensor head these nuts are the only metallic components of the force sensor. The finger fixation can be changed and adapted to the experimental requirements. 3D-printing of the PLA structure takes 45 min, and after further arrangement steps such as attaching the mirror, fitting the brass nuts and the silicon tube, the sensor can be calibrated and ready for use within less than 90 min following initialization of the fabrication process.

IV. Characterization

Several experiments were performed in order to characterize the dynamic behavior of the force sensor. Measurement data were collected using a commercial data acquisition (DAQ) card (NI USB 6008; National Instruments, USA). The resolution of this experimental setup (flexible structure, sensor head, analog amplifier, DAQ) was identified to be 0.01 N, which is higher than the force resolution of the human fingertip [20].

A. Sensitivity, Range, Linearity and Hysteresis

In a first experiment the sensitivity of the force sensor, its maximum range, linearity, and hysteresis error were investigated. The sensor was clamped into a vice and successively loaded with weights (forward measurement). Once the maximum weight was reached, it was successively unloaded back to zero (backward measurement). At each step of this process the output voltage of the analog amplifier was recorded. This procedure was repeated several times. As shown in Fig. 6, we found a highly linear behavior within the range of -2 N and 2 N, which is the region in which the deflecting probe can move freely. At higher forces the moving probe begins to contact the mechanical stops and the response is no longer linear. At ± 3 N the deflecting probe is in full contact with the mechanical stop and saturates. Within the linear range (R^2 value of 0.998), the sensitivity is 0.84 V/N. The hysteresis error (defined as the maximum vertical distance between the forward and backward measured voltage of the same weight) varied between 0.02 N and 0.14 N. From the endpoints of the linear range and the physically measured distance between deflecting probe and the mechanical stops (maximum free displacement) a stiffness of 0.075 mm/N was calculated, which corresponds well to the one identified by FEM analysis (0.08 mm/N).

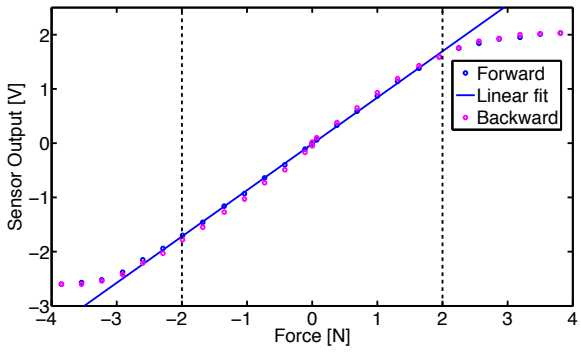

Fig. 6. Sensitivity characterization of the force sensor prototype: forward (loading) and backward (unloading) measurement. R^2 = 0.998.

B. Repeatability and Accuracy

In order to reliably detect forces the sensor must show a high repeatability (i.e. produce the same output voltage for the same force every time it is applied). Reliability was characterized by calculating the mean and average error of three data sets. In the linear range we found a mean absolute error of 0.03 V. Considering the previously identified sensitivity of 0.84 V/N, this yields an accuracy of approximately 0.03 N. Nevertheless, it has to be noted that here we do not include hysteresis errors (forward and backward measurement were treated separately and the sensor was recalibrated before each test).

C. Transverse Forces

As mentioned in section III-A, the rigidity of the elastic probe in the direction of the expected force is significantly lower than the rigidities along the other directions. However, the presented theory does not consider lever arms when force is applied on the sensor. For this reason, a further experiment investigated the sensitivity to transverse forces (forces perpendicular to the expected direction of force). The procedure was the same as in the previous experiments. The loads, however, were applied in four directions perpendicular to the expected direction of force, 10 mm away from the edge of the moving probe of the sensor. In the targeted application, the finger will also be placed about 10 mm from the sensor, hence the force was applied at this point. The sensitivity in each direction was calculated and compared to the sensitivity along the expected direction of force. The results are summarized in Table II.

D. Drift, Overload and Temporal Stability

Due to creep and relaxation of polymeric materials, we expected susceptibility of the deflecting structure to drift. This drift and the ability to recover were investigated. The sensor was loaded with a force of 1.5 N (mean value of full sensing range) for several hours, while the output voltage was recorded. Within the first few minutes the sensor drift was about 1% of the output voltage per minute and decreased as time progressed (Fig. 7, top), and only stopped when the mechanical stops were reached. Right after unloading the force sensor the recorded drift error was 0.5 N with no force applied. The recovery of the structure was faster in the beginning, with a final static error of 0.15 N (Fig. 7, bottom).

To simulate the response to maximum pinching forces, the sensor was loaded with 50 N force for 10 sec in a separate experiment, then released and loaded again after 10 sec. This procedure was repeated five times. We measured the hysteresis error at zero force before each loading cycle and found values in the same range as when small forces (between ± 3 N) were applied. This indicates that, thanks to the mechanical stops, no major plastic deformation (yield stress not reached) occurs in the flexible hinges when overloaded.

After the sensor was exposed to the drift and maximum overload experiments, the first experiment was repeated and the sensitivity was measured. Within the linear range the values of sensitivity (0.87 V/N), linear range (± 2 N), linearity (R^2 = 0.998) and hysteresis (0.08 N) were found to be unaffected (Fig. 8). This proves that the flexible structure can resist short overloads of 50 N entirely unaffected. It suffers, however, an offset, which can be removed through calibration.

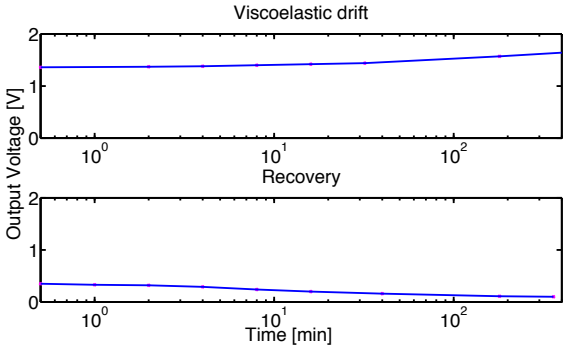

Fig. 7. Drift behavior over time of the force sensor. (top) Voltage output when a load of 1.5 N is applied for several hours. (bottom) Recovery of the structure after unloading.

Finally, another sensor sensitivity measurement was performed again after 6 months following initial experiments, and a maximum of 4% signal variation (0.16 N) was found within the linear range (± 2 N) when comparing to the initial dataset.

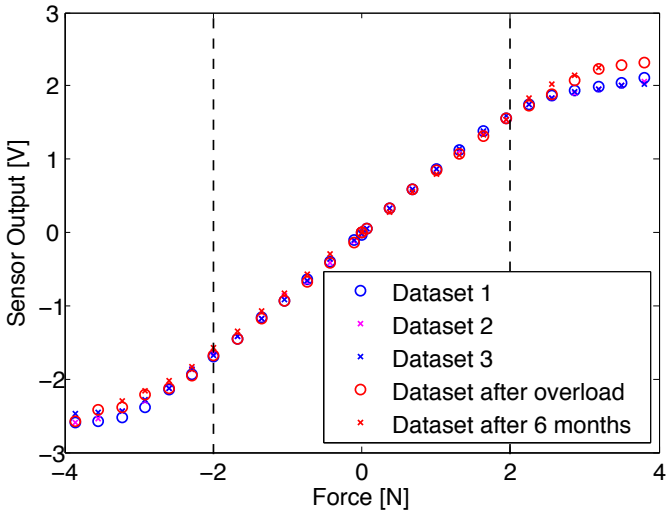

Fig. 8. Force sensor signal repeatability and reproducibility following drift and overload, as well as temporal stability. The sensor was loaded and unloaded 3 times sequentially (compression and tension; about 1 min duration per cycle; datasets 1–3), then overloaded with 50 N for 5 times (10 sec duration per cycle, with 110 sec of recovery between cycles), following which another complete load/unload cycle was performed (dataset after overload). An additional load/unload cycle of the same sensor probe was carried out 6 months after its production (dataset after 6 months). A maximum of 4% signal variation was found between the datasets.

E. Reproducibility

One of the greatest advantages of 3D printing is the short fabrication time. Nevertheless, this should be accompanied

by a reproducible behavior of the printed structures. We investigated this by comparing the range and linearity of four different sensor prototypes (Fig. 9). Inconsistent ROM of the deflecting probe induced by printing accuracy limitations lead to variations in the full sensor range (the deflecting probe contacts with the mechanical stops at different points). Nonetheless, within the linear range (where the deflecting part can move freely) all sensors perform highly similar. Reproducibility was demonstrated by measuring the repeatability between different 3D-prints according to the procedure described in subsection IV-B. The mean absolute error between the four 3D-prints was found to be 0.08 V ($\approx$ 0.07 N) within the linear range. Thus, different 3D-prints can be used interchangeably with an accuracy of 0.07 N. A

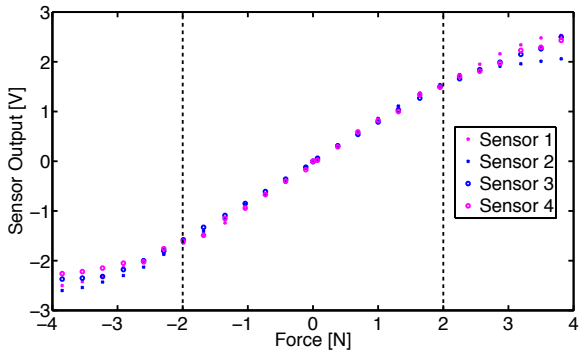

Fig. 9. Comparison of the force-voltage relation for four different 3D-prints of the same prototype. The maximum signal variation between the four sensors was found to be 5% (0.2 N), while the mean absolute error was calculated at 1.75% (0.07 N).

summary of the force sensor characteristics can be found in table II.

TABLE II

FIBEROPTIC SENSOR CHARACTERISTICS.

Range	-3 *N* – 3 *N*
Linear range	-2 *N* – 2 *N*
Sensitivity	0.84 *V/N*
Resolution	0.01 *N*
Linearity	0.9995 (R^2 value)
Stiffness	0.075 *mm/N*
Maximum stress	45% of yield stress
Maximum displacement	0.15 *mm*
Size	30.5 × 32.8 × 11.3 mm^3
Vertical transverse force sensitivity (up/down)	7% / 9% of normal sensitivity
Horizontal transverse force sensitivity (left/right)	19% / 19% of normal sensitivity
Maximum hysteresis	7% of range
Drift	1% of load per minute

F. Representative Application

To evaluate the developed sensor in a force-feedback scenario, it was integrated into a one-degree-of-freedom linear grasping device (Fig. 10). The device allows grasping motion between the thumb, which is fixed to the device structure, and the index finger, which is attached to a movable cart sliding on a linear friction guide. The cart is actuated by a direct-drive DC motor via a closed-loop cable drive. Two grasping experiments were performed in order to evaluate the performance of the sensor in a representative application, i.e. to measure the static friction in the rail and transmission, and to integrate it in a force feedback loop to improve device transparency. The first experiment consisted in a subject performing sinusoidal grasping movements (flexion and extension of the index finger), while the motor was turned off and the interaction force measured by the sensor was recorded. During the second experiment, the subject performed the same grasping movements, while the device rendered a virtual spring. Both experiments were carried out twice, without and with force feedback. Interaction forces during the four experiments are plotted in Fig. 11. During transparency rendering, the interaction force was reduced by a factor of three, from approximately 1.5 *N* to approximately 0.5 *N*. This was also observed during the rendering of a virtual spring, in which the large hysteresis loop could also be reduced by the same factor.

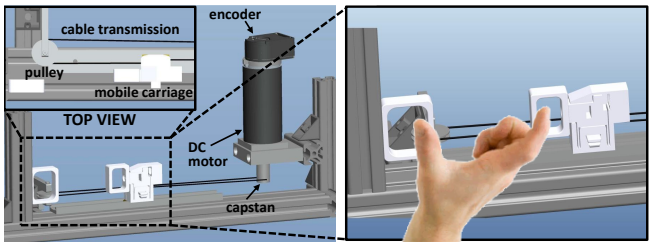

Fig. 10. One-degree-of-freedom linear grasping device with the force sensor integrated in the index finger fixation.

V. DISCUSSION AND CONCLUSION

We presented a compact, small-range fMRI-compatible force sensor based on fiberoptics and fabricated using low-cost 3D printing. The sensor presents a high linearity with a low hysteresis error, the force detection is highly repeatable, while its elastic probe can be manufactured with a high reproducibility and temporal stability, displaying a high accuracy (0.07 N or 1.75% of the sensor range -2 to 2 N) when compared to similar sensors (2-4% of 0–10 N, [21]). The sensor resolution is above the human fingertip force resolution and it can sustain short overloads in the range of the maximum pinching force without notable changes in its characteristics. Besides the sensor's main advantage of cost and time efficient fabrication, it contains very little metal (non-magnetic brass) and its design can be adapted quickly to individual applications and to integrate surrounding mechanical components. This includes the adaptation of the sensing range by changing the dimensions of the flexible hinges (following equations 1–7).

One limitation of the proposed force sensor is its susceptibility to drift, an acknowledged characteristic of the PLA material, and accepted as a trade-off for fMRI-compatibility. Additionally it is sensitive to transverse forces, however, in an acceptable range. The offset caused by drift can be

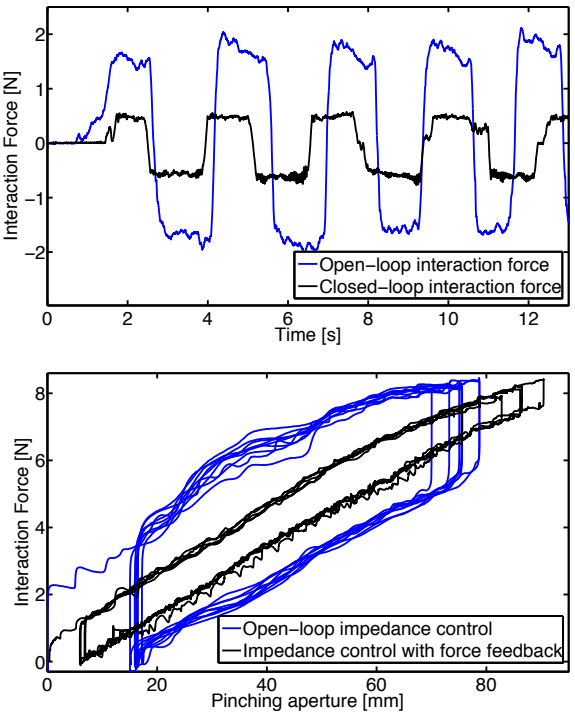

Fig. 11. Interaction force during rendering of transparency (top) and a virtual spring (bottom).

minimized by calibrating the sensor before every use. Thanks to its high linearity, two recorded voltage outputs of two discrete force loads are sufficient for the calibration. To address the sensitivity to transverse forces, further mechanical stops or a more conservative design of the flexible hinges (higher rigidities in directions perpendicular to the desired force direction) could be considered.

The sensor size is constrained by the limitations of the 3D printer. Despite its high nozzle positioning precision (0.011 mm), the minimum layer thickness of 0.1 mm and the nozzle diameter of 0.4 mm affected the resolution and printing accuracy. These are non-negligible limitations considering the maximal mirror-displacement of 0.6 mm, particularly for sensors designed for small force ranges. Nonetheless, these drawbacks are overcome by the advantages these fabrication technologies bring in terms of fast and affordable production. Moreover, force sensors can be directly printed into the surrounding structure, as shown in our finger pinching application, which further demonstrates the feasibility of using the proposed sensor in force-feedback applications.

REFERENCES

[1] J. Diedrichsen, Y. Hashambhoy, T. Rane, and R. Shadmehr, "Neural correlates of reach errors," *The Journal of Neuroscience*, vol. 25, no. 43, pp. 9919–9931, 2005.

[2] R. Gassert, L. Dovat, O. Lambercy, Y. Ruffieux, D. Chapuis, G. Ganesh, E. Burdet, and H. Bleuler, "A 2-DOF fMRI compatible haptic interface to investigate the neural control of arm movements," in *Proceedings of the IEEE International Conference on Robotics and Automation (ICRA)*, 2006, pp. 3825–3831.

[3] R. Gassert, R. Moser, E. Burdet, and H. Bleuler, "MRI/fMRI-compatible robotic system with force feedback for interaction with human motion," *Mechatronics, IEEE/ASME Transactions on*, vol. 11, no. 2, pp. 216–224, 2006.

[4] N. Yu, W. Murr, A. Blickenstorfer, S. Kollias, and R. Riener, "An fmri compatible haptic interface with pneumatic actuation," in *Proceedings of the IEEE International Conference on Rehabilitation Robotics (ICORR)*, 2007, pp. 714–720.

[5] A. Hribar and M. Munih, "Development and testing of fmri-compatible haptic interface," *Robotica*, vol. 28, no. 02, pp. 259–265, 2010.

[6] J. Izawa, T. Shimizu, T. Aodai, T. Kondo, H. Gomi, S. Toyama, and K. Ito, "Mr compatible manipulandum with ultrasonic motor for fmri studies," in *Proceedings of the IEEE International Conference on Robotics and Automation (ICRA)*, 2006, pp. 3850–3854.

[7] S. Menon, G. Brantner, C. Aholt, K. Kay, and O. Khatib, "Haptic fmri: Combining functional neuroimaging with haptics for studying the brain's motor control representation," in *Proceedings of the 37th Annual Conference of the IEEE Engineering in Medicine and Biology Society (EMBC)*, 2013, pp. 4137–4142.

[8] R. Gassert, D. Chapuis, H. Bleuler, and E. Burdet, "Sensors for applications in magnetic resonance environments," *Mechatronics, IEEE/ASME Transactions on*, vol. 13, no. 3, pp. 335–344, 2008.

[9] J. Liu, T. Dai, T. Elster, V. Sahgal, R. Brown, and G. Yue, "Simultaneous measurement of human joint force, surface electromyograms, and functional mri-measured brain activation," *Journal of Neuroscience Methods*, vol. 101, no. 1, pp. 49–57, 2000.

[10] J. Hidler, T. Hodics, B. Xu, B. Dobkin, and L. G. Cohen, "Mr compatible force sensing system for real-time monitoring of wrist moments during fmri testing," *Journal of Neuroscience Methods*, vol. 155, no. 2, pp. 300–307, 2006.

[11] S. Hirose and K. Yoneda, "Development of optical six-axial force sensor and its signal calibration considering nonlinear interference," in *Proceedings of the IEEE International Conference on Robotics and Automation (ICRA)*, 1990, pp. 46–53.

[12] M. Tada, S. Sasaki, and T. Ogasawara, "Development of an optical 2-axis force sensor usable in mri environments," in *Proceedings of IEEE Sensors*, vol. 2, 2002, pp. 984–989.

[13] J. Arata, S. Terakawa, H. Fujimoto, J. Sulzer, and R. Gassert, "Mri-compatible grasping force sensor with an inclined double parallel structure using fiber optics," in *Proceedings of the ASME/ISCIE International Symposium on Flexible Automation*. American Society of Mechanical Engineers, 2012, pp. 77–82.

[14] H. Xie, A. Jiang, H. Wurdemann, H. Liu, L. Seneviratne, and K. Althoefer, "Magnetic resonance-compatible tactile force sensor using fiber optics and vision sensor," *IEEE Sensors Journal*, 2014.

[15] D. Chapuis, R. Gassert, L. Sache, E. Burdet, and H. Bleuler, "Design of a simple mri/fmri compatible force/torque sensor," in *Proceedings of the IEEE/RSJ International Conference on Intelligent Robots and Systems (IROS)*, vol. 3, 2004, pp. 2593–2599.

[16] M. Hara, J. Duenas, T. Kober, D. Chapuis, O. Lambercy, H. Bleuler, and R. Gassert, "Design and compatibility of a high-performance actuation system for fmri-based neuroscience studies," in *Proceedings of the IEEE/RSJ International Conference on Intelligent Robots and Systems (IROS)*, 2010, pp. 2437–2442.

[17] B. Buchholz, L. J. Frederick, and T. J. Armstrong, "An investigation of human palmar skin friction and the effects of materials, pinch force and moisture," *Ergonomics*, vol. 31, no. 3, pp. 317–325, 1988.

[18] S. Henein, *Conception des guidages flexibles*. PPUR presses polytechniques, 2001.

[19] F. Rezgui, M. Swistek, J. Hiver, C. G'sell, and T. Sadoun, "Deformation and damage upon stretching of degradable polymers (pla and pcl)," *Polymer*, vol. 46, no. 18, pp. 7370–7385, 2005.

[20] E. S. Dellon, R. Mourey, and A. L. Dellon, "Human pressure perception values for constant and moving one-and two-point discrimination," *Plastic and reconstructive surgery*, vol. 90, no. 1, pp. 112–117, 1992.

[21] S. B. Kesner and R. D. Howe, "Design principles for rapid prototyping forces sensors using 3-d printing," *Mechatronics, IEEE/ASME Transactions on*, vol. 16, no. 5, pp. 866 – 870, 2011.